Title: “DistorX” program for analysis of structural distortions affecting X-ray diffraction patterns

Author: Lech Kalinowski, Jerzy Goraus, Andrzej Ślebarski

Citation style: Kalinowski Lech, Goraus Jerzy, Ślebarski Andrzej. (2018). “DistorX” program for analysis of structural distortions affecting X-ray diffraction patterns. “AIP Advances “ (vol. 8 (2018), Art. No. 101334), doi 10.1063/1.5042654

"DistorX" program for analysis of structural distortions affecting X-ray diffraction patterns

L. Kalinowski,[1,2,a] J. Goraus,[2] and A. Ślebarski[2]
[1]*Future Processing, ul. Bojkowska 37A, 44-100 Gliwice, Poland*
[2]*Institute of Physics, University of Silesia, ul. 75 Pułku Piechoty 1A, 41-500 Chorzow, Poland*

(Received 3 June 2018; accepted 1 October 2018; published online 12 October 2018)

For the purposes of research on strongly correlated electronic systems (SCES), a computer program, DistorX (Distortion or X-ray diffraction patterns), was created. The program is an interactive Jupyter notebook for simulating the effects of structural distortions on X-ray diffraction patterns. The program is designed to be universal, in that it may be successfully applied to a variety of structures. In previous reports, a structural transition from a cubic phase of $Yb_3Rh_4Sn_{13}$ – type to the superlattice variant was been observed at 160 K for a series of skutterudite-related $Ce_3M_4Sn_{13}$ compounds, where M = Co, Ru or Rh. In this work, we use a specialized build of DistorX to simulate the low-temperature X-ray diffraction patterns of a distorted unit cell. The method described here obtains simulated XRD patterns from the atomic positions and permits investigation of crystal structure without imposed symmetry operations. We further indicate the crystallographic plane in which the distortion occurs, and explain the possible origin of CDW in these materials.
https://doi.org/10.1063/1.5042654

I. INTRODUCTION

Filled skutterdites with a chemical formula $R_3M_4Sn_{13}$, where R is rare earth atom, and M is Co, Ru or Rh, have been extensively investigated due to their diverse heavy fermion properties and interesting interplay between superconductivity, magnetic order and thermoelectric properties, which are closely related to the cage-type structure.[1] The Sn1-ions form a bcc structure in the $Yb_3Rh_4Sn_{13}$ - type compounds. Each Sn1 atom is surrounded by 12 pnictogen Sn2 ions, forming a slightly distorted icosahedron, and eight transition elements forming a cube. Each atom M is located inside an $M(Sn2)_6$ trigonal prism, while each atom R is at the center of an $R(Sn2)_{12}$ cuboctahedron. Recent density functional calculations[2] showed high charge density accumulation between metal M and Sn2 atoms, which implies a strong covalent bonding interaction. It has been shown[6] that even a small change of local symmetry, such as distortion of the $M(Sn2)_6$ and $R(Sn2)_{12}$ cages generated by a small deformation of the Sn_{12} icosachedra, can lead to variation in the charge density of metal M and R ions. The slight structural deformation of the $R(Sn2)_{12}$ cage also changes the symmetry of the crystal electric field (CEF), which is observed in the specific heat and magnetic susceptibility data.[3] Generally, the strong covalent bonding in R-based skutterudite-related compounds may be a key mechanism responsible for the variety of unusual properties.[4] In particular, the heavy fermion properties for R=Ce, superconductivity with novel structural quantum critical point (QCP) for R=La[5] and strong electronic correlation have attracted considerable attention due to the electronic structure and cage-type crystal structure. Detailed investigations and empirical analyses suggest that structural distortion, which is observed at about $T_D \sim 160$ K in most of these compounds, has a strong influence on the electronic structure of the system.[6] Strongly correlated electronic systems (SCES), such as

[a]Electronic mail: lechkalinowski@gmail.com

$Ce_3Co_4Sn_{13}$, experience charge density waves with accompanying structural distortions.[7] Here, we compare the low temperature x-ray diffraction patterns to DistorX simulations, considering structural distortion caused by a charge density wave. This structural phase transition has also been observed recently at $T_D \sim 160$ K for other $Ce_3Ru_4Sn_{13}$ and $Ce_3Rh_4Sn_{13}$ compounds,[8] similar to CDW-type ordering suggested by Song et al. 2003.[9] We further investigate the effect of CDW structural change on diffraction patterns of $Ce_3M_4Sn_{13}$. This procedure allows comparison and verification of a model structure to experimental data. We also determine the crystallographic planes responsible for the structural distortion in $R_3M_4Sn_13$, assuming that the amplitude of CDW may be a cause of structural disorder. The observed structural disorder appears to be essential to understanding the competition between superconductivity and CDW in the family of La-based $R_3M_4Sn_{13}$ compounds,[10] as well as the nature of structural quantum phase transitions at $T_D \rightarrow 0$.

II. EXPERIMENTAL DETAILS

Polycrystalline samples $Ce_3M_4Sn_{13}$, M=Co, Ru and Rh, have been prepared by arc melting of the pure elements in a water-cooled copper hearth, in a high-purity argon atmosphere with an Al getter. Samples were annealed at 870^oC for 14 days. All samples were characterized by X-ray-diffraction analysis at room temperature, confirming a single phase with a cubic structure ($Pm\bar{3}n$). Low temperature x-ray diffraction was performed using a high-resolution diffractometer (Empyrean PANalitical B. V. with TTK 450 Anton-Paar detector). Stoichiometry of the samples was checked by x-ray fluorescence spectrometry (ZSX Primus II Rigaku) and X-ray photoelectron spectroscopy (PHI 5700 ESCA spectrometer).

III. CDW SIMULATION METHOD

Optimization of the input structure was based on the Hellmann-Feynman theorem,[11] applied with a DFT calculation method. The structures were visualized using VESTA.[12] XRD Ritveld analysis was performed using Xpert High Score Plus.

XRD simulations are based on Bragg, Laue's and Fourier's theoretical basis of solid state physics. The DistorX program used to simulate XRD patterns was written in Python 2.7[13] using, "numpy" and "matplotlib"[14] libraries. The visualization module[15] was also useful for identification of atomic positions and modeling of CDW distortion. All dependent modules are open-source Python scripts connected in a Jupyter notebook web-app environment to manage simulation results. DistorX is published in an on-line repository.[16] Line profile was introduced as a Pseudo-Voigdt distribution function. XRD patterns simulated with DistorX were compared against those obtained with other software packages, namely: Full Prof package, Powder Cell and Mercury. All mentioned programs give exact the same result of simulated $Ce_3M_4Sn_{13}$ (M=Co, Ru, Rh) XRD patterns.

Experimental diffraction patterns were refined by the Ritveld method for all samples at 300 K and 85 K. The results are presented in Table I. Refined lattice parameters are used in the CDW distortion simulation.

The model implies a change in positions of atoms across the c crystal axis. Changes in the local environment of the R atom lead to a strong reconstruction of the Fermi level and the electronic structure, as was shown in previous reports.[6,18] We assumed the presence of charge accumulation in the (0 0 1) planes near Ce atoms, which we implemented as a primitive unit cell with a doubled lattice

TABLE I. The lattice parameters of $Ce_3Co_4Sn_{13}$, $Ce_3Ru_4Sn_{13}$ and $Ce_3Rh_4Sn_{13}$, respectively, and the obtained R_{Bragg} factors.

Compound	T [K]	a [Å]	$2a$ [Å]	R_{Bragg}
$Ce_3Co_4Sn_{13}$	300	9.5949	19.1898	13.5
	85	9.5677	19.1355	14.4
$Ce_3Ru_4Sn_{13}$	300	9.7249	19.4498	6.2
	85	9.7009	19.4018	6.0
$Ce_3Rh_4Sn_{13}$	300	9.5958	19.1917	11.9
	85	9.5679	19.1359	12.8

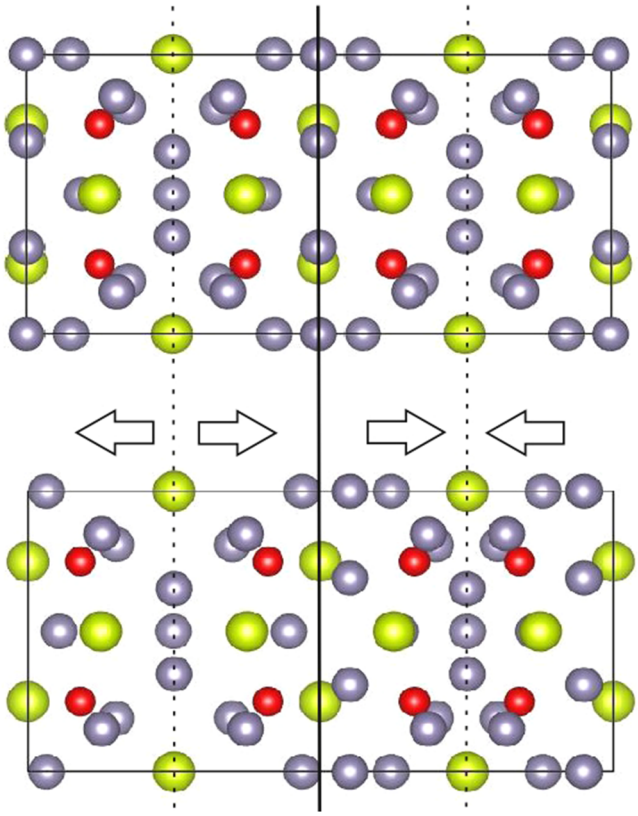

FIG. 1. Visualization of doubled unit cell of $Ce_3M_4Sn_{13}$ (M=Co, Ru, Rh) after optimization with selected symmetry axis. Arrows indicate the direction of deformation caused by CDW. Green spheres represents Ce atoms, red spheres corresponds to metal M, and gray spheres represent Sn1 and Sn2 atoms.

parameter, c. The distortion also explains the observed super-lattice peaks in the XRD patterns. In that case, two Ce atoms are located directly in the middle of the modified unit cell. We modeled the distortion using

$$Z_N(i) = Z(i) + A\cos(2\pi Z(i)), \tag{1}$$

where, $Z_N(i)$ represents new z Cartesian coordinate of i^{th} atom, $Z(i)$ is the nominal z coordinate of an atom, and A is the amplitude of the charge density wave. Fig. 1 shows the structure deformation direction for the modified unit cell. In this model, the Ce-atom positions are fixed, while M and Sn atoms have one unconstrained degree of freedom and can be shifted. Our program generates XRD patterns directly from the Cartesian (x, y, z) positions of atoms, treating input structures as having $P1$ symmetry. This allows us to study structures without imposing symmetry operations and thus allowing generation of diffraction patterns with arbitrary distortions.

Atomic form factors were applied as a function of tabulated parameters a_n of x-ray scattering ability of elements.[17] Structure factors were calculated to obtain the intensities of the diffraction lines, where the structural F-factor is multiplied by the Lorentz polarization factor.

IV. RESULTS AND DISCUSSION

The simulation is obtained on the optimized and doubled unit cell with applied CDW distortion, giving an additional $2\theta \sim 24.3^o$ reflection, which is not present in other simulated patterns generated from the base atomic Wyckoff positions with applied symmetry operations. This superlattice diffraction line is consistent with the XRD pattern obtained at temperatures lower than T_D at $2\theta < 40^o$ diffraction angles. This result is further consistent with the presence of a superlattice variant with a double c lattice parameter seen in experimental data, and may confirm that the structural phase

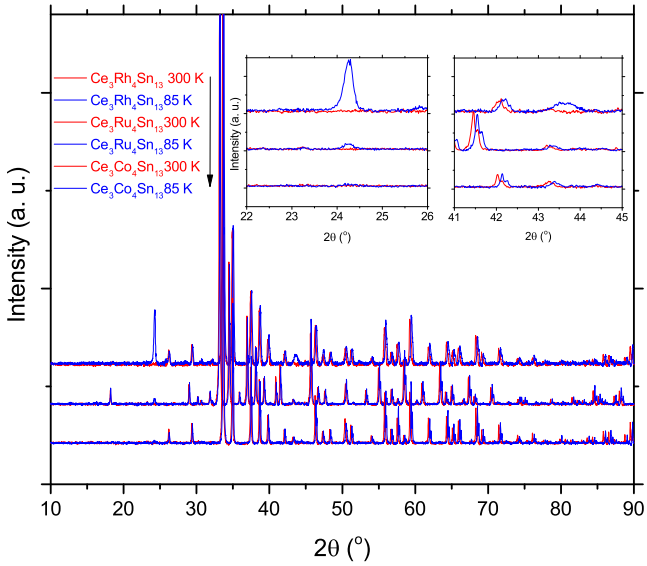

FIG. 2. XRD experimental diffraction patterns for $Ce_3Co_4Sn_{13}$, $Ce_3Ru_4Sn_{13}$ and $Ce_3Rh_4Sn_{13}$ at 300 K and 85 K. Insets show detailed areas where the superlattice peaks arise.

transition is caused by a charge density wave. The distortion lattice plane in $Ce_3Rh_4Sn_{13}$ visible in the low temperature diffraction pattern was also corroborated by DistorX simulations. Fig. 2 compares the XRD patterns measured for $Ce_3Co_4Sn_{13}$, $Ce_3Ru_4Sn_{13}$, and $Ce_3Rh_4Sn_{13}$, respectively, at $T = 300$ K and $T = 85$ K. At 85 K, the additional peak is clearly visible in all the diffraction patterns at $2\theta \sim 24.2^o$. Moreover, the change of its intensity is strongly M dependent, and has a maximum value for Rh. In the case of $Ce_3Rh_4Sn_{13}$, the XRD pattern at 85 K exhibits another diffraction line at $2\theta \sim 43.6^o$. These diffraction patterns are in good agreement with the simulation of the CDW distorted structure with an amplitude between $A = 0.01$ Å and $A = 1$ Å with $A = 0.001$ Å step. Experimental and simulated intensities are normalized to 1. Change of the distortion amplitude leads to a change in the peaks intensities. Moreover, for A larger then 1 Å the $2\theta \sim 24.2^o$ diffraction line disappears.

In Fig. 3 the black pattern represents a structure with amplitude $A = 0$ Å, i.e., without distortion, whereas the green pattern represents a distorted structure with $A = 0.05$ Å. We noticed

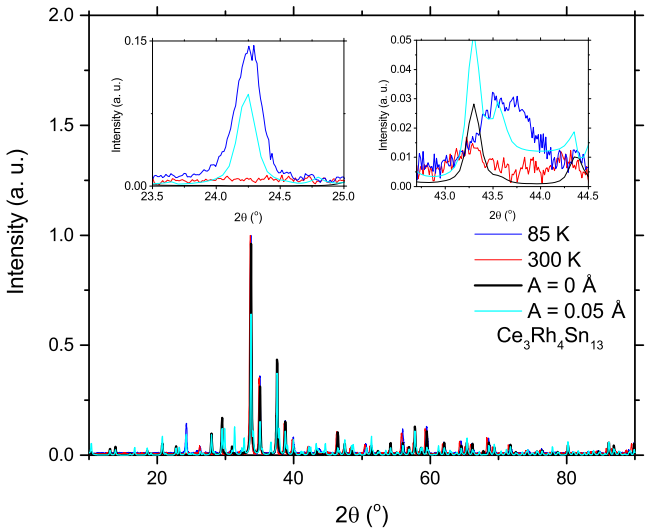

FIG. 3. XRD experimental diffraction pattern for $Ce_3Rh_4Sn_{13}$ at 300 K and 85 K, compared with simulation of CDW distortion. Insets display region where superlattice peaks appear.

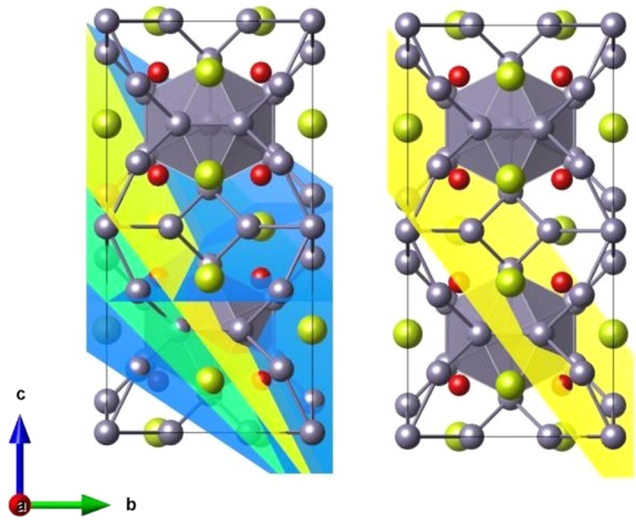

FIG. 4. Visualization of $Ce_3M_4Sn_{13}$ (M=Co, Ru, Rh) after optimization with marked lattice planes (1 1 2), (0 2 2) green color, (0 1 5), (1 0 5), (2 1 3) - blue color, and (1 2 3) - yellow color. Color spheres represent atoms described in fig. 1.

that CDW structural distortion generates a new peak located in the XRD diffraction pattern at about $2\theta = 24.2^o$, which is not resolved by Ritveld analysis for the base unit cell. For amplitude $A = 0.05$ Å the simulation peak intensity has the best match with experiment. In the commercial program Xpert High Score Plus, the Ritveld analysis of experimental pattern implies weak diffraction lines at $2\theta = 22.7^o$ (1 1 2), $2\theta = 26.3^o$ (0 2 2), which are barely seen experimentally. For a simulated distortion at $2\theta = 24.2^o$, DistorX designates equivalent lattice planes (0 1 5) (1 0 5) (2 1 3) visible in fig. 4 as blue and the (1 2 3) plane (yellow). Plane (1 2 3) is most likely related to a structural phase transition. This plane is located between (1 1 2) and (0 2 2) lattice planes, as shown in fig. 4. It intersects icosahedron cages between Sn1-Sn2 atoms. Moreover, M atoms lie in this plane. Previous reports[18] clearly indicate charge accumulation inside the cages, and a charge deficit is directly observed on transition metal M. Both effects lead to deformation of the cages. An accompanying subtle structural distortion changes the symmetry of the crystal electric field. The CEF symmetry is lower than cubic, which is well documented by specific heat and magnetic susceptibility data.[6]

V. CONCLUSIONS

Experimental low-temperature x-ray diffraction studies of $Ce_3M_4Sn_{13}$ demonstrated the presence of a structural phase transition at ~160 K from a cubic $Pm\bar{3}n$ structure to its superlattice variant. We simulated X-ray diffraction patterns using DistorX and compared the simulations with experimental low-temperature XRD data. We demonstrated that the distortion established by charge density accumulation creates additional diffraction peaks, in agreement with experimental XRD patterns. We have also shown which planes are more likely to be distorted. Our previous DFT results[18] indicated the impact of the f-electron and d-electron correlations on the charge distribution in the unit cell of $Ce_3M_4Sn_{13}$. For M = Co, a significant loss of spatial charge on metal M is documented, which is weaker for Rh, in contrast to a positive charge accumulation observed for Ru. Moreover, for M=Co or M=Rh, the Sn2 cages accumulate inside most of the charge between Sn1 and Sn2 atoms. As a result, the charge accumulation leads to strong covalent bonding. This bonding between M and Sn1 further leads to strong distortion in $Ce_3M_4Sn_{13}$, as manifested in the XRD patterns. Both the charge accumulation in the cages and the charge deficit on the transition metal M give rise to a charge density wave that leads to the distortion of positions of atoms and a shift in position of transition metal M. We showed that the direction of charge density wave propagation is not associated with any preferred crystallographic axis (a, b, c), and may arise along the lattice planes (1 2 3) where effect of the charge accumulation on the atoms is most significant.

SUPPLEMENTARY MATERIAL

Please see supplementary material for the full DistorX Python computer code.

ACKNOWLEDGMENTS

We thank the National Science Centre Poland for financial support No. UMO-2014/15/N/ST3/03799. We thank NVIDIA Corporation for the donation of a Titan Xp GPU.

[1] B. Maple, J. Phys. Soc. Jpn. **74**, 222 (2005).
[2] M. Gamża, W. Schnelle, A. Ślebarski, U. Burkhardt, R. Gumeniuk, and U. Rosner, J. Phys.: Condens. Matter **20**, 395208 (2008).
[3] A. Ślebarski, B. D. White, M. Fijałkowski, J. Goraus, J. J. Hamlin, and M. B. Maple, Phys. Rev. B **86**, 205113 (2012).
[4] T. Goto, Y. Nemoto, K. Onuki, K. Sakai, T. Yyamaguchi, M. Akatsu, T. Yanagisawa, H. Sugawara, and H. Sato, J. Phys. Soc. Jpn. **74**, 263 (2005).
[5] L. E. Klintberg, S. K. Goh, P. L. Aliveza, P. J. Saines, D. A. Tompsett, P. W. Logg, J. Yang, B. Chen, K. Yoshimura, and F. M. Grosche, Phys. Rev. Lett. **109**, 237008 (2012).
[6] A. Ślebarski, M. Fijałkowski, J. Goraus, L. Kalinowski, and P. Witas, J. Alloys Compd. **615**, 921 (2014).
[7] C. S. Lue, H. F. Liu, S.-L. Hsu, M. W. Chu, H. Y. Liao, and Y. K. Kuo, Phys. Rev. B **85**, 205120 (2012).
[8] A. Ślebarski and J. Goraus, Phys. Rev. B **88**, 155122 (2013).
[9] C. Song, J. Park, J. Koo, K.-B. Lee, J. Y. Rhee, S. L. Bud'ko, P. C. Canfield, B. N. Harmon, and A. I. Goldman, Phys. Rev. B **68**, 035113 (2003).
[10] C. A. Balseiro and L. M. Falicov, Phys. Rev. B **20**, 11 (1979).
[11] Q. Wu and T. Van Voorhis, Phys. Rev. A **72**, 024502 (2005).
[12] K. Momma and F. Izumi, J. Appl. Crystallogr. **41**, 653 (2008).
[13] Python Software Foundation (2001-2006), Python Language Reference version 2.7., Available at http://www.python.org.
[14] J. D. Hunter, Comp. Sci. Eng. **9**, 90 (2007).
[15] D. Scherer, P. Dubois, and B. Sherwood, Comp. Sci. Eng. **2**, 56 (2000).
[16] L. Kalinowski (2017), Google Sites DistorX v2.3, https://sites.google.com/smcebi.edu.pl/distorx.
[17] P. J. Brown, A. G. Fox, E. N. Maslen, M. A. O'Keefe, and B. T. M. Willis, International Tables for Crystallography C **6**(1), 554–595 (2006).
[18] A. Ślebarski, J. Goraus, and P. Witas, Phys. Rev. B **92**, 155136 (2015).